J Mater Sci: Mater Electron (2015) 26:1649–1660
DOI 10.1007/s10854-014-2589-4

Interfacial reaction and mechanical properties between low melting temperature Sn–58Bi solder and various surface finishes during reflow reactions

Sang-Min Lee · Jeong-Won Yoon · Seung-Boo Jung

Received: 12 September 2014 / Accepted: 6 December 2014 / Published online: 18 December 2014
© Springer Science+Business Media New York 2014

Abstract Interfacial reactions and joint mechanical reliability of a representative low melting temperature Sn–58 wt%Bi solder with three different surface finishes were evaluated during a reflow process. The surface materials consisted of organic solderability preservative (OSP), electroless nickel–immersion gold (ENIG), and electroless nickel–electroless palladium–immersion gold (ENEPIG). The relationships between the interfacial reaction, surface finish, shear speed, and shear force were elucidated in this study. The interfacial intermetallic compounds (IMCs) on the ENEPIG substrate were sequentially changed during reflowing at 180 °C in the following order: $(Pd,Ni)Sn_4$, $(Pd,Ni)Sn_4 + Ni_3Sn_4$, and Ni_3Sn_4. Compared to the Cu_6Sn_5 IMC on the OSP-finished Cu substrate, the Ni_3Sn_4 IMCs on the ENIG and ENEPIG substrates were much thinner. The IMCs of each of the different surface finishes grew as the reflow time increased; however, the morphologies of the IMCs were different each other. Layer-type interfacial IMCs created a stable metallurgical interfacial structure during the reflow reaction, resulting in reduced rates of IMC growth and Ni–P consumption. High-speed shear tests were conducted to evaluate the effects of interfacial reactions on the mechanical properties of three Sn–58Bi solder joints. In spite of the different interfacial reactions and IMC formations, there were no large differences among shear forces in the three Sn–58Bi solder joints. Further, the type of surface finish material did not significantly affect the shear force of the Sn–58Bi solder joints under high-speed shear loading.

S.-M. Lee
SKKU Advanced Institute of Nanotechnology (SAINT), Sungkyunkwan University, 300 Cheoncheon-dong, Jangan-gu, Suwon, Gyeonggi-do 440-746, Korea

J.-W. Yoon (✉)
Micro-Joining Center, Korea Institute of Industrial Technology, 156 Gaetbeol-ro, Yeonsu-gu, Incheon 406-840, Korea
e-mail: jwyoon@kitech.re.kr

S.-B. Jung (✉)
School of Advanced Materials Science and Engineering, Sungkyunkwan University, 300 Cheoncheon-dong, Jangan-gu, Suwon, Gyeonggi-do 440-746, Korea
e-mail: sbjung@skku.edu

1 Introduction

Solder joints are an indispensable part of electronic packaging technology, as they maintain both the mechanical stability of packages while simultaneously delivering both electrical signals and thermal energy from devices. The reliability and strength of solder joints generally depends on the interfacial structures between metallization and lead (Pb)-free solder. During the soldering process, solder alloy melts and reacts with metallization of the substrate to form intermetallic compounds (IMCs) at the joint interface. The formation of an IMC layer between the substrate metal and the molten solder is generally created to obtain a sufficient metallurgical bond and to guarantee electrical and thermal conduction, although excessive IMC formation may result in brittle failure [1, 2]. Therefore, the surface finish should be able to produce a reliable solder joint when assembled at a high temperature with a Pb-free solder. The selection of an appropriate barrier metal such as a surface finish depends on cost, availability, and compatibility with existing materials as well as the manufacturing processes for conventional electronic packaging industry. Among the many available surface finishes, organic solderability preservative (OSP)-finished Cu and electroless nickel–immersion gold (ENIG) are well-known and very versatile.

Specifically, these finishes provide solderable surfaces with an excellent shelf life and excellent electrical contacting surfaces. In addition to OSP and ENIG, electroless nickel–electroless palladium–immersion gold (ENEPIG) represents the finish with the widest range of applications. ENEPIG was originally introduced in the mid-90s, but did not capture a significant share of the market due to its incompatibility with conventional Sn–Pb solder [3]. However, the Pb-free restriction of hazardous substances (RoHS) requirement has made it necessary to once again revisit all available surface finishes, and ENEPIG has again come under close scrutiny as the industry evaluates its capabilities using Pb-free assembly conditions [4].

The electronic industry relies on Pb-free solders because of the harmful effects lead can have on the environment and human health. One of the important requirements for electronics solders is processing temperature as low as, or lower than Sn–Pb solder. Therefore, a representative low-temperature Pb-free solder, Sn–58 wt%Bi solder, is nominated as substitutable solder. The low melting point of this solder makes it suitable for soldering temperature-sensitive components and substrates.

Several studies on the interfacial reactions between Pb-free solders and various surface finishes of ENIG [5–8], ENEPIG [9–15], and OSP-finished Cu [16–19] have been performed. Nevertheless, data and reports on the effects of ENEPIG surface finish on interfacial reactions and joint reliability are seriously lacking, especially for joints utilizing Sn–58Bi solder. Therefore, in this study, we performed a comparative study of the characteristics and interfacial IMC formation of Sn–58Bi solder joints containing OSP, ENIG, or ENEPIG. The corresponding mechanical reliability was measured by a bump shear test.

2 Experimental procedures

The solder composition used in this study was a eutectic Sn–58Bi (in wt%) solder. The substrate was a solder mask defined-type flame retardant-4 (FR-4) laminate with subsurface solder bond pads whose nominal size and shape were defined through a 200 µm-diameter circular opening. Three kinds of surface finishes were used in this study, namely, electroless nickel–immersion gold (ENIG, 7 µm Ni–P/0.1 µm Au), electroless nickel–electroless palladium–immersion gold (ENEPIG, 7 µm Ni–P/0.1 µm Pd/0.1 µm Au), and organic solderability preservative (OSP). The electroless Ni–P layer contained about 15 at.% P due to the use of hypophosphite in the chemical reaction for reducing Ni ions.

The Sn–58Bi solder paste was applied by stencil printing method and the subsequent reflow was carried out in an IR four zone reflow machine (RF-430-Ne, Japan Pulse Laboratory Co. ltd). The peak temperature was maintained at 180 °C and the dwell times at the peak temperature were either 45, 80 s, 30 min, or 1 h. After soldering, the diameter and height of the formed solder bumps were approximately 250 and 150 µm, respectively. A reflow time longer than 10 min is generally unnecessary for industrial applications; however, in the present study, we evaluated reflow times up to 1 h. The main purpose of using this unrealistic reflow time was to investigate the distinguishable interfacial reaction between Sn–58Bi solder and various substrate materials. In addition, we were interested in ensuring that the reaction products were thick enough for subsequent analyses.

Interfacial microstructures and IMC morphologies were observed by scanning electron microscopy (SEM, Hitachi S-3000H), and the compositions of IMCs were determined by energy dispersive X-ray spectroscopy (EDX). The thickness of the interfacial IMC layer was evaluated using image analysis software to measure the total area of the intermetallic layer. To determine average layer thicknesses, phase areas were divided by the interface length depicted in cross-sections. In order to determine the effect of surface finish material and interfacial reaction during reflow reaction on the mechanical properties of Sn–58Bi solder joints, high-speed shear tests were conducted using a global bond tester (DAGE-4000HS, Nordson). We evaluated shear speeds of 0.01, 0.1, and 0.5 m/s with a fixed shear height of 30 µm. A total of 20 solder bumps were tested at each condition and the average values were reported.

3 Results and discussion

Figure 1 shows cross-sectional SEM images of Sn–58Bi/OSP-finished Cu joints reflowed at 180 °C for different reflow times. Interfacial reactions of this type of solder joint are well-known in the field of electronic materials, and we used this type of solder joint as a base-line for comparison with other types of surface finish materials. The microstructure of the Sn–58Bi solder consisted of a Bi-rich phase (white phase) and an Sn-rich phase (grey phase) as shown in Fig. 1. In the case of the OSP surface finish, Cu_6Sn_5 IMC was formed at the interface, and as shown in Fig. 1a the interface between the Cu_6Sn_5 IMC and solder had a scalloped morphology. In the joint reflowed for 45 s, the thickness of the Cu_6Sn_5 IMC layer was approximately 1 µm. The interfacial structure of the joint reflowed for 80 s, as shown in Fig. 1b, was similar to that of the sample reflowed for 45 s, and only scallop-type Cu_6Sn_5 IMC was detected at the interface. After reflowing for 30 min, a Cu_3Sn IMC was formed at the interface between the Cu_6Sn_5 layer and Cu substrate, as shown in Fig. 1c. Generally, Cu_6Sn_5 and Cu_3Sn are the

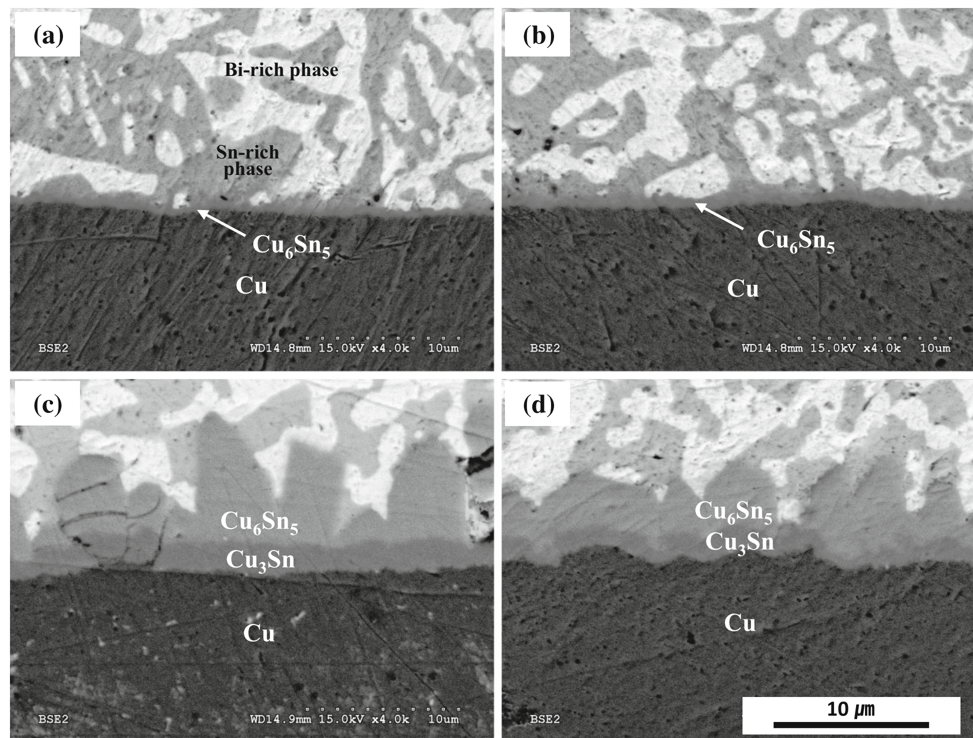

Fig. 1 Cross-sectional SEM images of the Sn–58Bi/OSP-finished Cu interfaces reflowed at 180 °C for various times: **a** 45 s, **b** 80 s, **c** 30 min, and **d** 1 h

main reaction products in this type of reaction couple [17]. In addition, most Sn-based solder alloys form these two reaction layers at the interface between the solders and Cu. The thickness of the two IMC layers Cu_6Sn_5 and Cu_3Sn increased with increasing reflow time. Specifically, the thicknesses of the combined Cu–Sn, Cu_6Sn_5, and Cu_3Sn IMCs in the joint reflowed for 1 h were approximately 6, 4 and 2 µm, respectively. The Sn–58Bi/OSP-finished Cu joint reflowed for 1 h consisted of the Cu substrate, Cu_3Sn IMC layer, Cu_6Sn_5 IMC layer, Bi-rich phase, and the Sn-rich phase shown in Fig. 1d.

A top view observation was performed to evaluate the effect of reflow time on the morphology of the IMCs formed between the Sn–58Bi solder and OSP-finished Cu substrate. Figure 2 shows the top view SEM images of the interfacial IMCs formed at the Sn–58Bi/OSP-finished Cu interface for different reflow times. As reflow time increased, the shape of IMCs changed from a scallop shape to a facet shape. A small scallop shaped Cu_6Sn_5 was initially formed for 45 s and the IMCs grew and enlarged for 80 s. After reflowing for 30 min, scallop-shaped Cu_6Sn_5 IMCs were changed into facet shaped IMCs. In addition, the size of IMCs increased with increasing reflow time. The results of the interfacial structures from the top view SEM micrographs of Fig. 2 were consistent with the cross-sectional images shown in Fig. 1.

Figure 3 shows the cross-sectional SEM images of the Sn–58Bi/ENIG joints reflowed at 180 °C for different reflow times. During initial reflowing, the entire Au layer on the Ni–P layer dissolved into molten solder and the Sn–Bi solder formed only Ni_3Sn_4 IMC at the solder/Ni–P interface (Fig. 3a). After reflowing for 80 s, a P-rich Ni (hereafter Ni_3P) layer formed at the interface between Ni_3Sn_4 and electroless Ni–P layer. This Ni_3P layer contained approximately 25 at.% P. Due to the consumption of Ni in the electroless Ni–P layer to form the interfacial Ni_3Sn_4 IMC, P is expelled to the remaining Ni–P layer and forms an Ni_3P layer [8]. Consistent with this observation, there was a weak contrast boundary line between the thin Ni_3P layer and the Ni–P layer as shown in Fig. 3b. After reflowing for 30 min, the Ni_3Sn_4 and Ni_3P layers thickened. In addition, a distinct phase containing Sn, Ni and P formed in between the Ni_3Sn_4 and Ni_3P layers. This ternary Ni–Sn–P layer was confirmed as Ni_2SnP, consistent with our previous transmission electron microscopy (TEM) study [20]. The thickness of the Ni_3Sn_4 IMC layer increased with increasing reflow time. Even when the reflow time was prolonged up to 1 h, only the Ni_3Sn_4 IMC layer was observed at the Sn–Bi/ENIG interface as shown in Fig. 3d. The thickness of the Ni_3Sn_4 IMC in the joint reflowed for 1 h was approximately 3 µm. On the other hand, the thickness of original Ni–P plating layer

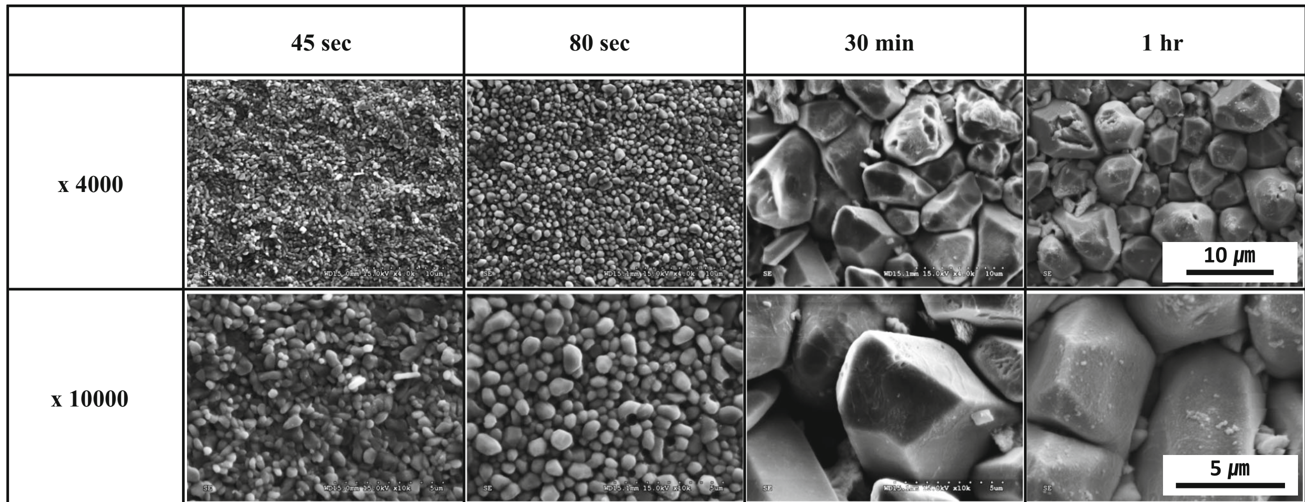

Fig. 2 Top view SEM images of IMCs formed at the Sn–58Bi/OSP-finished Cu joints for different reflow times

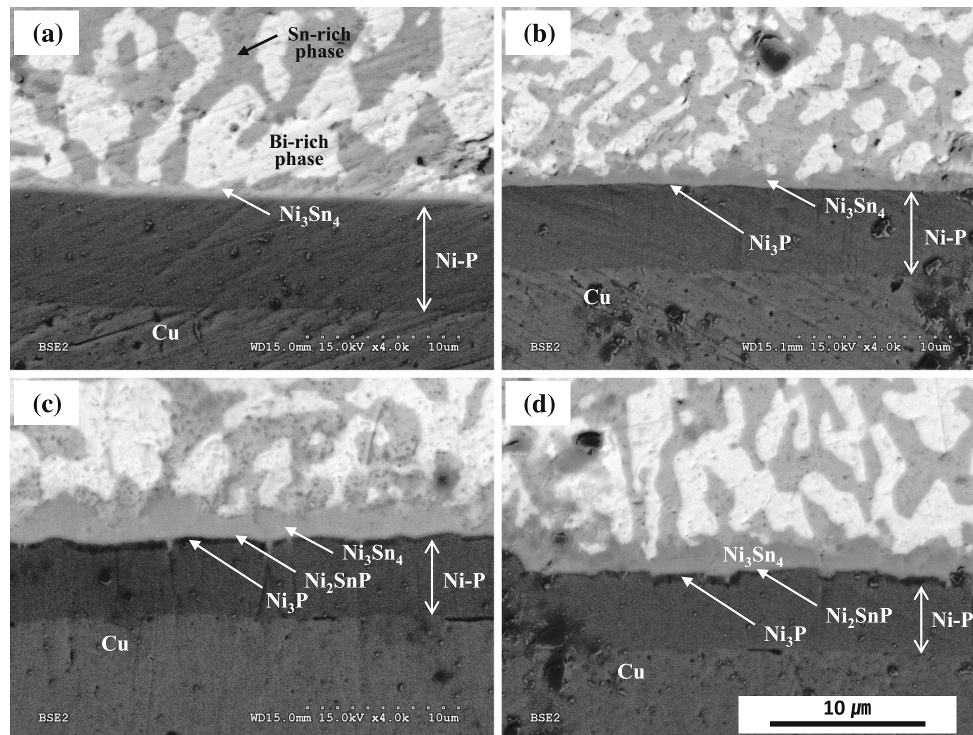

Fig. 3 Cross-sectional SEM images of the Sn–58Bi/ENIG interfaces reflowed at 180 °C for various times: **a** 45 s, **b** 80 s, **c** 30 min, and **d** 1 h

decreased. The remaining Ni–P layers were indicated with white arrows in Fig. 3. As a whole, a relatively thin and continuous Ni_3Sn_4 IMC layer was present at the Sn–58Bi/ENIG interface. Compared to the Cu_6Sn_5 IMC on the OSP-finished Cu substrate, the Ni_3Sn_4 IMC on the ENIG substrate was much thinner.

Figure 4 shows the top view SEM images of the interfacial IMCs formed at the Sn–58Bi/ENIG joint for different reflow times. As the reflow time increased, the morphology of the Ni_3Sn_4 IMC changed from a needle shape to chunky shape. Similar results have been reported in the literature [6, 21].

A markedly different morphology was observed from the reflow of the Sn–58Bi solder on the ENEPIG substrate. Figure 5 shows the cross-sectional SEM images of the Sn–58Bi/ENEPIG joints reflowed at 180 °C for different reflow times. During the initial reflow reaction, the outermost Au layer of the ENEPIG layer dissolved into molten

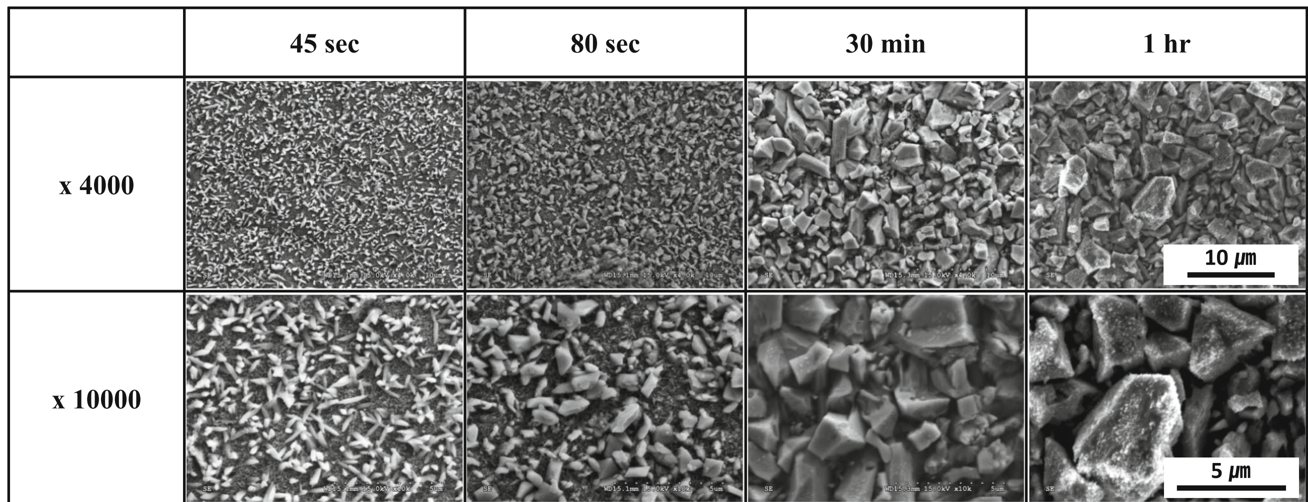

Fig. 4 Top view SEM images of IMCs formed at the Sn–58Bi/ENIG joints for different reflow times

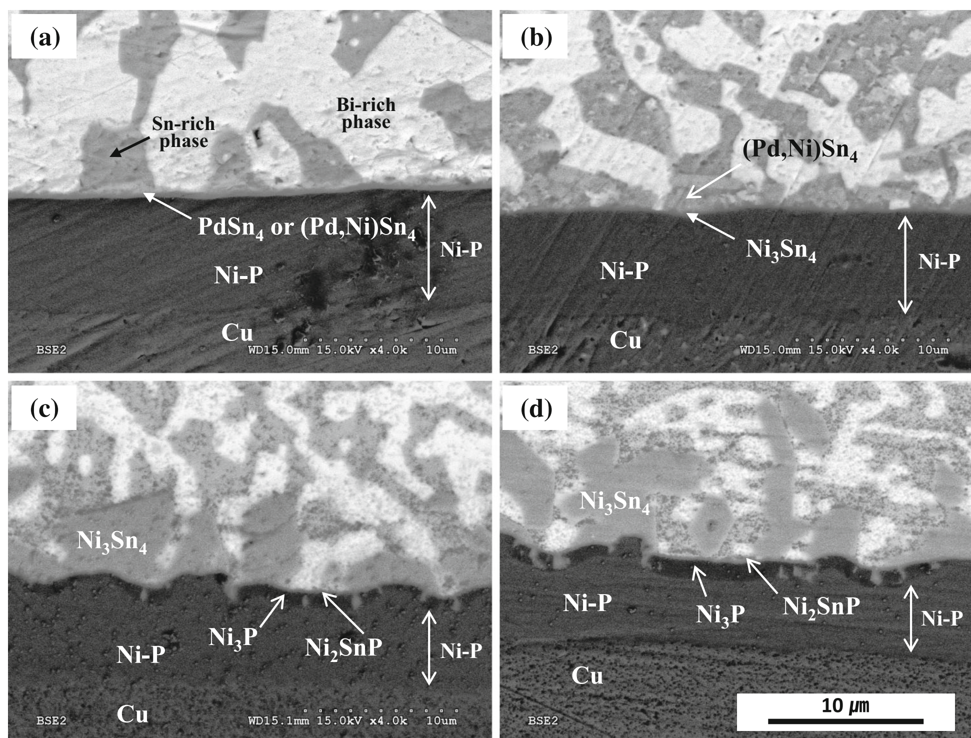

Fig. 5 Cross-sectional SEM images of the Sn–58Bi/ENEPIG interfaces reflowed at 180 °C for various times: **a** 45 s, **b** 80 s, **c** 30 min, and **d** 1 h

solder and Sn–Bi solder reacted with the Pd layer to form $PdSn_4$ or $(Pd,Ni)Sn_4$ IMC at the solder/Ni–P interface (Fig. 5a). Several researchers have reported the presence of $PdSn_4$ or $(Pd,Ni)Sn_4$ IMC [22, 23]. Ni atoms diffused into the substitutional sites of Pd atoms in the $PdSn_4$ IMC, resulting in the formation of $(Pd,Ni)Sn_4$ IMC. After reflowing for 80 s, two IMCs, namely $(Pd,Ni)Sn_4$ and Ni_3Sn_4, comprised the majority of IMCs as shown in Fig. 5b. The growth of $(Pd,Ni)Sn_4$ IMC stopped due to the limited Pd thickness of the ENEPIG substrate. In addition, Ni_3Sn_4 IMC formed underneath the $(Pd,Ni)Sn_4$ IMC. A similar result has been reported in the literature [24]. Peng et al. reported the formation and sequential spalling of $(Pd,Ni)Sn_4$ IMC of a Sn–37Pb/Au/Pd/Ni(P) joint during a reflow reaction at 220 °C.

During reflowing for 30 min, the formed $(Pd,Ni)Sn_4$ IMCs were completely dissolved into the molten solder, and Ni_3Sn_4 IMC formed at the interface as shown in

Fig. 5c. In addition, the Ni_3Sn_4 IMC was not layer-structure and had chunky-type morphology. Furthermore, the Ni_3P and Ni_2SnP layers formed on the Ni–P layer. The Ni_3P layer is not continuous. We found the relatively bright parts in the dark Ni_3P layer. Indeed, these parts are destroyed Ni_3P parts due to the prolonged reflow reaction [25]. After reflowing for 1 h, the spalling of Ni_3Sn_4 IMC was accelerated as shown in Fig. 5d. In addition, molten solder directly contacted the interface in many parts. As a result, there were numerous bright parts in the dark Ni_3P layer. The thickness of the Ni_3P layer increased with increasing reflow time.

Figure 6 shows top view SEM images of the IMCs formed at the Sn–58Bi/ENEPIG joints. Until reflowing for 80 s, fine needle-shape $PdSn_4$ or $(Pd,Ni)Sn_4$ IMCs formed at the interface, and grew with reflow time. As the reflow time increased up to 1 h, faceted rod-shape Ni_3Sn_4 IMCs formed at the interface.

We next performed a quantitative analysis of the IMC thickness as a function of the reflow time. Figures 7, 8 and 9 show the thicknesses of the IMC layers formed at the Sn–58Bi/OSP-finished Cu, Sn–58Bi/ENIG, and Sn–58Bi/ENEPIG interfaces as a function of reflow time, respectively. The thickness of the IMC layers increased with reflow time. Relatively thick interfacial IMC layers were formed at the Sn–58Bi/OSP-finished Cu joint. The results of this study clearly demonstrated the advantages of ENIG and ENEPIG substrates with respect to ensuring the interfacial stability of Sn–58Bi solder joints from the total IMC thickness. On the other hand, there was no significant difference between ENIG and ENEPIG. One interesting feature of this study was that the Sn–58Bi/ENEPIG joints exhibited slightly higher growth rates of the Ni_3Sn_4 IMC and Ni_3P layers than the Sn–58Bi/ENIG joint. We also

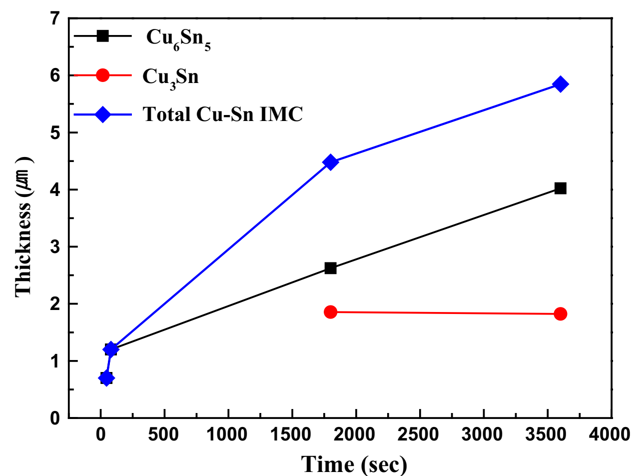

Fig. 7 Interfacial IMC thickness of the Sn–58Bi/OSP-finished Cu joints according to reflow time

investigated the interfacial reactions of Sn–3.0Ag–0.5Cu/ENIG and Sn–3.0Ag–0.5Cu/ENEPIG joints during the reflow reaction, which we compared with a set of previous results [26] to provide a direct comparison between the Sn–58Bi and Sn–3.0Ag–0.5Cu joints.

Figure 10 shows a comparison of results between Sn–58Bi and Sn–3.0Ag–0.5Cu joints. The Sn–3.0Ag–0.5Cu joints were reflowed at 260 °C due to their higher melting temperature. In the study, we found that the Sn–Ag–Cu/ENIG joint exhibited a higher IMC growth rate as well as a higher rate of consumption of the Ni–P layer than the Sn–Ag–Cu/ENEPIG joint. It is also known that the presence of a thin Pd layer of the ENEPIG substrate effectively suppresses both the growth of interfacial IMC layers and the consumption of the Ni–P layer in the Sn–Ag–Cu/ENEPIG joint [26]. However, in this study, we obtained the opposite

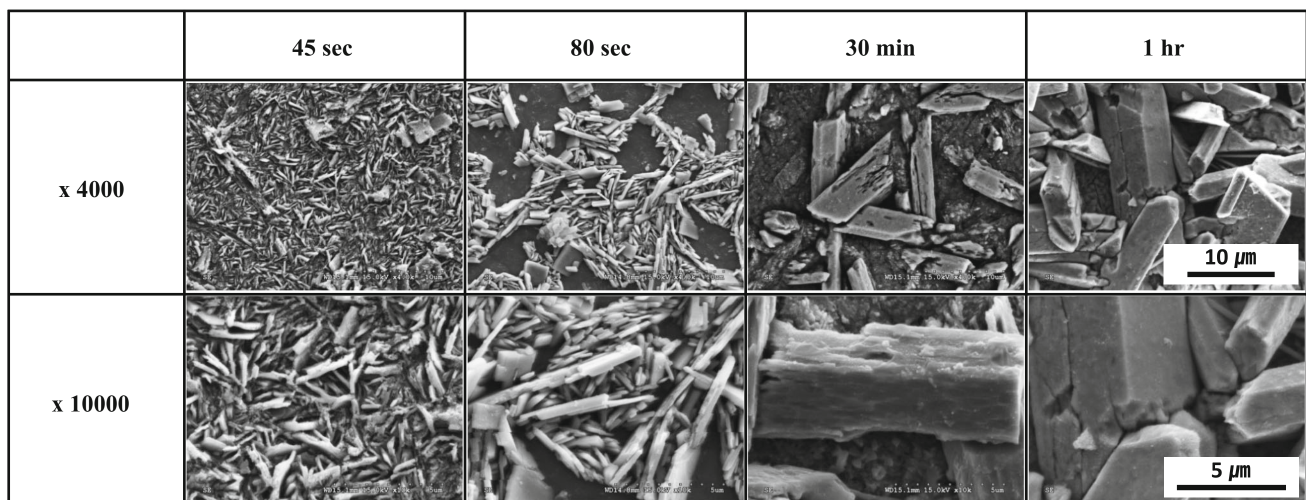

Fig. 6 Top view SEM images of IMCs formed at the Sn–58Bi/ENEPIG joints for different reflow times

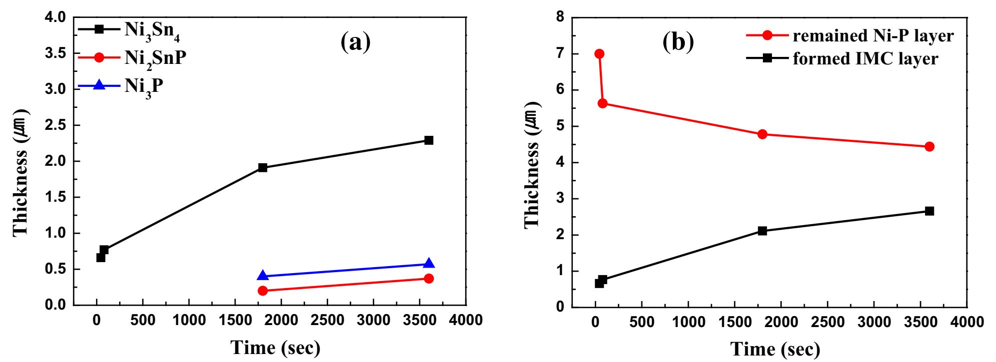

Fig. 8 **a** Interfacial IMC thickness and **b** remaining Ni–P layer thickness of the Sn–58Bi/ENIG joints according to reflow time

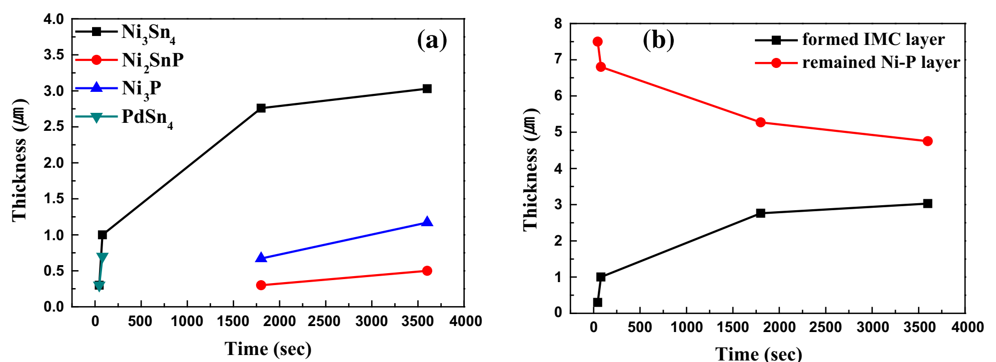

Fig. 9 **a** Interfacial IMC thickness and **b** remaining Ni–P layer thickness of the Sn–58Bi/ENEPIG joints according to reflow time

result for the Sn–58Bi solder system. Specifically, the growth rate of the interfacial IMC layer and consumption rate of the Ni–P layer were closely related to the interfacial microstructure and morphology. In the case of the Sn–58Bi/ENIG joint, the Ni_3Sn_4 IMCs were well attached at the interface and the thin Ni_3P layer formed on the Ni–P layer. On the other hand, in the case of the Sn–58Bi/ENEPIG joint, many Ni_3Sn_4 IMCs spalled from the interface, which resulted in the formation of a thick Ni_3P layer on the Ni–P layer. Opposite results were obtained in the Sn–Ag–Cu system as shown in Fig. 10, suggesting that the layer-type and well-attached interfacial IMCs were advantageous with respect to IMC growth rate and Ni–P layer consumption. Indeed, once the stable layer-type interfacial IMCs formed at the interface during the reflow reaction, the interfacial IMC layer effectively protected the subsequent accelerated reaction between liquid solder and the solid substrate. Although the exact reasons for the different interfacial reactions and interfacial microstructure with different solder system are not clear at this point, it is presumably related to the discrepancy of reflow temperature, the rate of Pd dissolution into the molten solder, and Pd solubility in the Sn–Ag–Cu solder and Sn–Bi solder. These results clearly indicated that the compatibility between solder materials and surface finishes was very important in terms of solder interfacial reactions and interfacial stability.

In order to evaluate the effect of surface finish and interfacial reaction on the mechanical properties of Sn–58Bi solder joints, high-speed shear tests were conducted. Figures 11 and 12 show the shear force variation of the Sn–58Bi solder joints with different surface finishes and reflow time under high-speed shear tests. The shear force exhibited a strong tendency to shear speed in the high-speed shear test. As shown in Fig. 11, the shear force increased with increasing shear speed to a maximum at the highest shear speed regardless of different surface finishes and reflow time. The shear forces measured by the high-speed shear loading (0.5 m/s) were higher than those of the low-speed shear loading (0.01 m/s), indicating that the increase in shear force with increasing shear speed was a direct consequence of material properties, including both time-independent plastic hardening and time-dependent strain-rate sensitivity [27]. Thus, the shear force increased with increasing shear speed, and resistance to plastic deformation increased with increasing impacted shear displacement rate.

An interesting phenomenon was observed in the high-speed shear test. Specifically, in samples reflowed for 45 s, the Sn–58Bi/ENEPIG joint had the lowest shear force value as shown in Figs. 11a and 12c. On the other hand, the Sn–58Bi/ENEPIG joints had the highest shear force values among the samples reflowed for 30 min and 1 h as shown in Fig. 11c, d. This variation in shear force was attributed

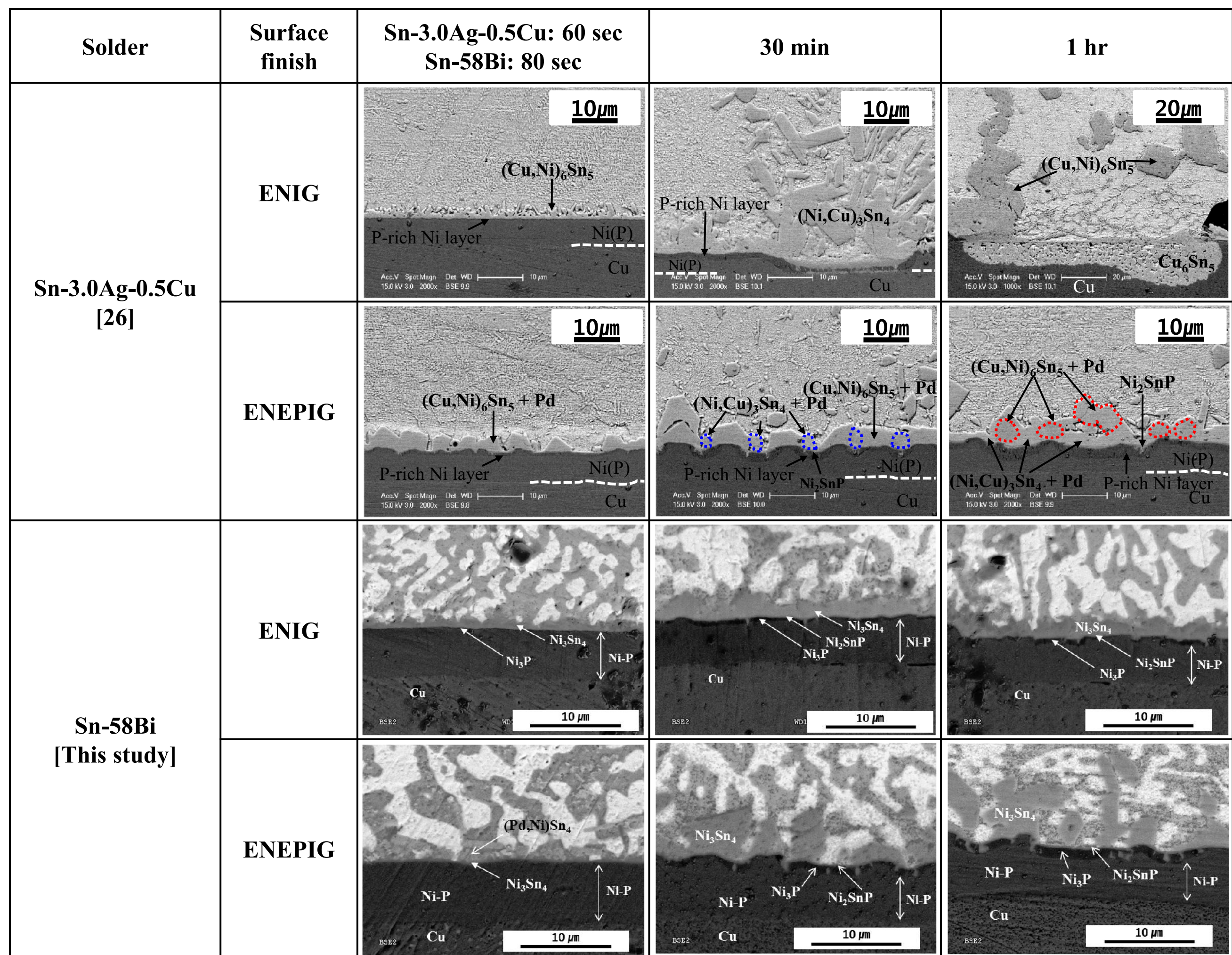

Fig. 10 Comparison between Sn–3.0Ag–0.5Cu solder [26] and Sn–58Bi solder (this study)

to the transition of the interfacial IMCs that formed. As mentioned above, the (Pd,Ni)Sn_4 IMC was initially formed at the Sn–58Bi/ENEPIG joint. During the prolonged reflow reaction, the Pd layer was completely consumed, and the Ni_3Sn_4 IMC formed at the interface. As a result, the Sn–58Bi/ENEPIG joint with (Pd,Ni)Sn_4 IMC had a relatively low shear force. In contrast, the Sn–58Bi/ENEPIG joint with Ni_3Sn_4 IMC was robust and had a high shear force value. These differences in the shear force corresponded to the different fracture modes, and thus we next investigated the fracture surfaces after the high-speed shear test. Figure 13 shows the fracture surfaces of the Sn–58Bi solder joints with various substrates after shear testing at a high-speed of 0.01 m/s. A substantial interfacial brittle fracture occurred in the Sn–58Bi/ENEPIG joint reflowed for 45 s, and the interfacial fracture parts are indicated with white arrows in Fig. 13. On the other hand, ductile solder fractures were also observed in other joints. These results are consistent with the shear force results.

An interesting aspect of this study was that the surface finish materials did not significantly affect the shear force of the Sn–58Bi solder joints under high-speed shear loading. As shown in Fig. 11, the shear force for the three kinds of surface finishes had similar values at each shear speed condition regardless of reflow time. It is generally known that thick interfacial IMC layers deteriorated an interfacial reliability and decreased shear strength of solder joints. According to our previous study for SAC305 solder, the failure mode switched from a bulk solder failure to an interface failure mode, depending on the reflow time [26]. However, in this study, the shear strength and failure mode of Sn–58Bi solder joints were not significantly affected by reflow time.

Figure 14 shows the shear force–displacement (F–x) curves obtained from the high-speed shear test. As a whole, the surface finish variation did not significantly affect the behavior of the F–x curves. The overall shape of the F–x curves changed distinctly with varying

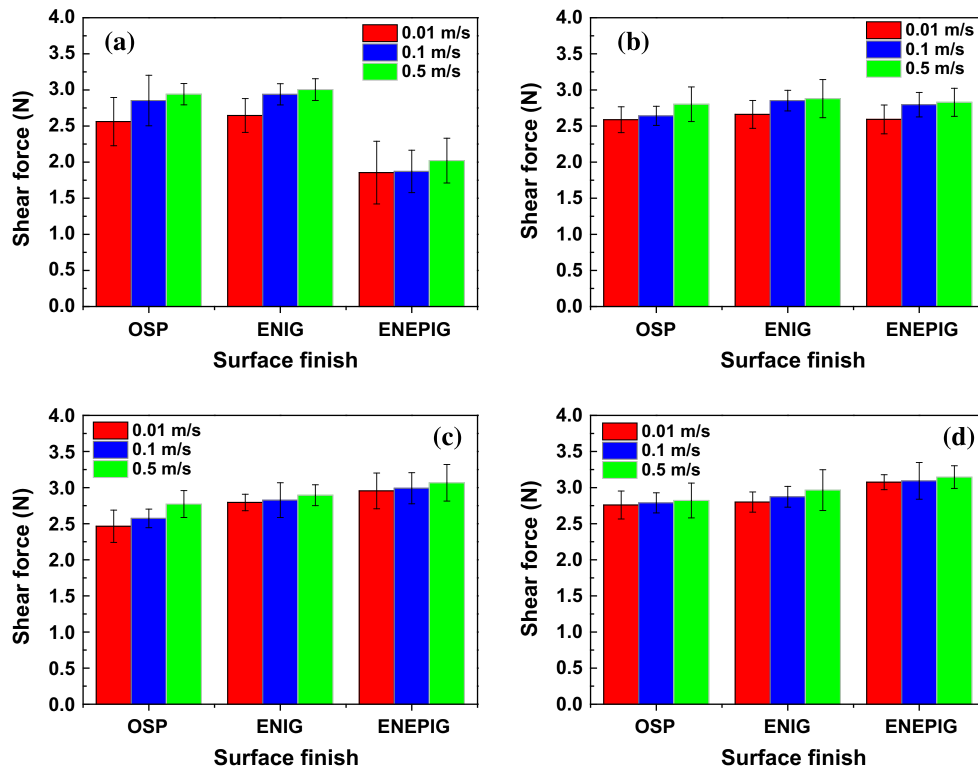

Fig. 11 Shear force variation with surface finish and shear speed: reflowed for **a** 45 s, **b** 80 s, **c** 30 min, and **d** 1 h

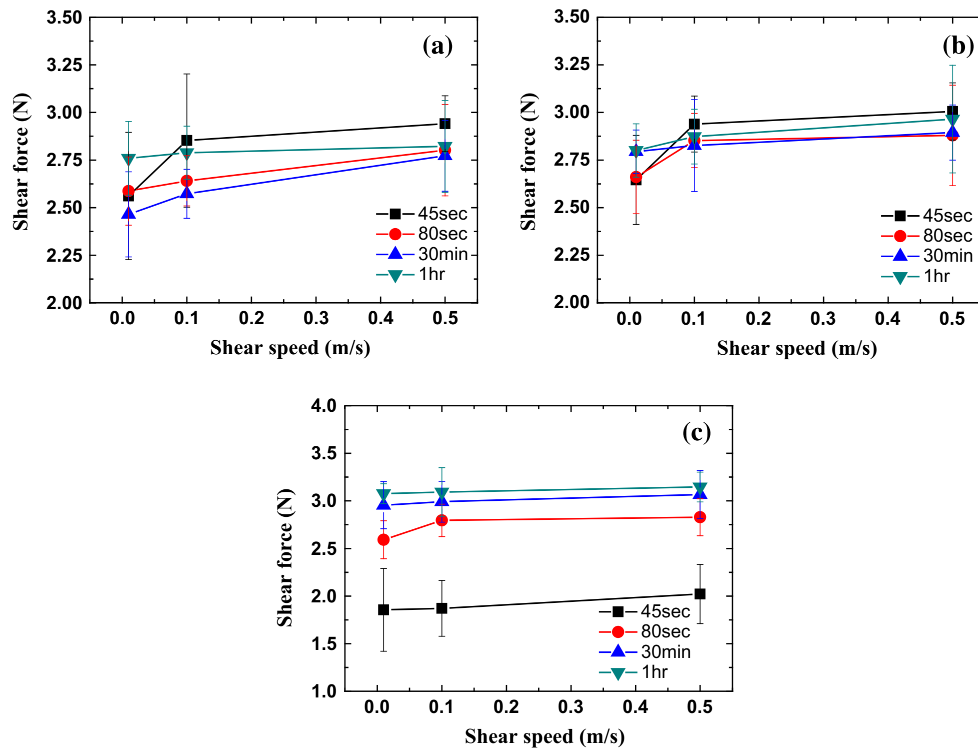

Fig. 12 Shear force variation according to shear speed: **a** OSP-finished Cu, **b** ENIG, and **c** ENEPIG

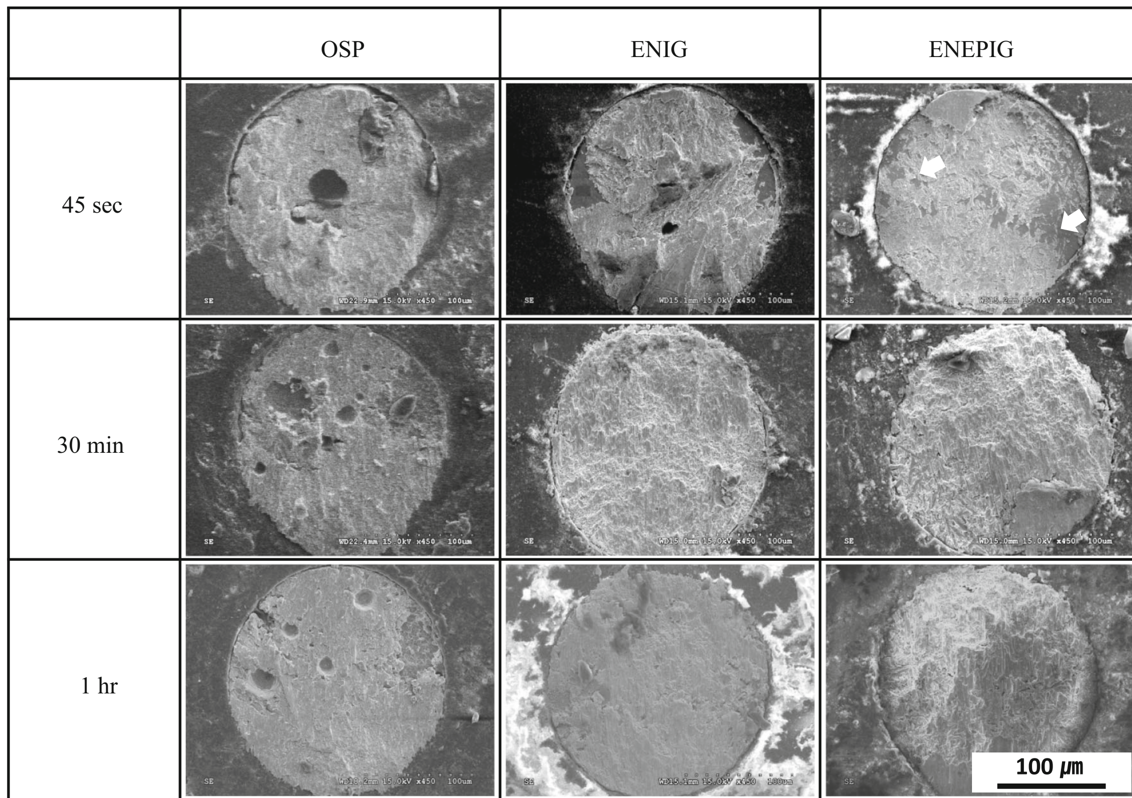

Fig. 13 Fracture surfaces of the Sn–58Bi/various substrate joints after shear testing at a high speed of 0.01 m/s

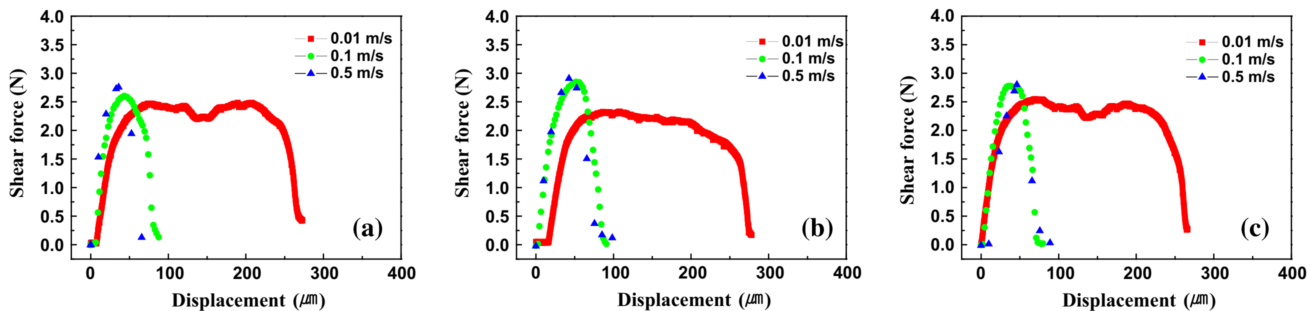

Fig. 14 Force–displacement (F–x) curves according to surface finish and shear speed (reflowed for 80 s): **a** OSP-finished Cu, **b** ENIG and **c** ENEPIG

loading speed regardless of surface finish materials. Furthermore, samples loaded at a lower loading speed (0.01 m/s) exhibited a large elongation followed by a gradual drop in flow stress before the stress progressed to a complete fracture (square symbols). In contrast, samples tested at higher loading speeds (0.1 and 0.5 m/s) produced somewhat different shaped flow stress curves, in that the elongation was smaller and the stress dropped sharply and immediately after peaking (circle and triangle symbols). In the latter case, the stress increased sharply and dropped abruptly with almost no plastic deformation. Although not presented here, the F–x curves for the joints reflowed for other reflow times exhibited similar characteristics to those described above for the joints reflowed for 80 s.

We next calculated the fracture energy of the high-speed shear test from the F–x curves: fracture energy corresponds to the area below F–x curves. Figure 15 shows the calculated fracture energies for different surface finishes and shear speeds. The sample with the lowest shearing speed had the highest fracture energy due to its large elongation properties. On the other hand, the sample with the highest shearing speed had the lowest fracture energy due to its poor elongation properties.

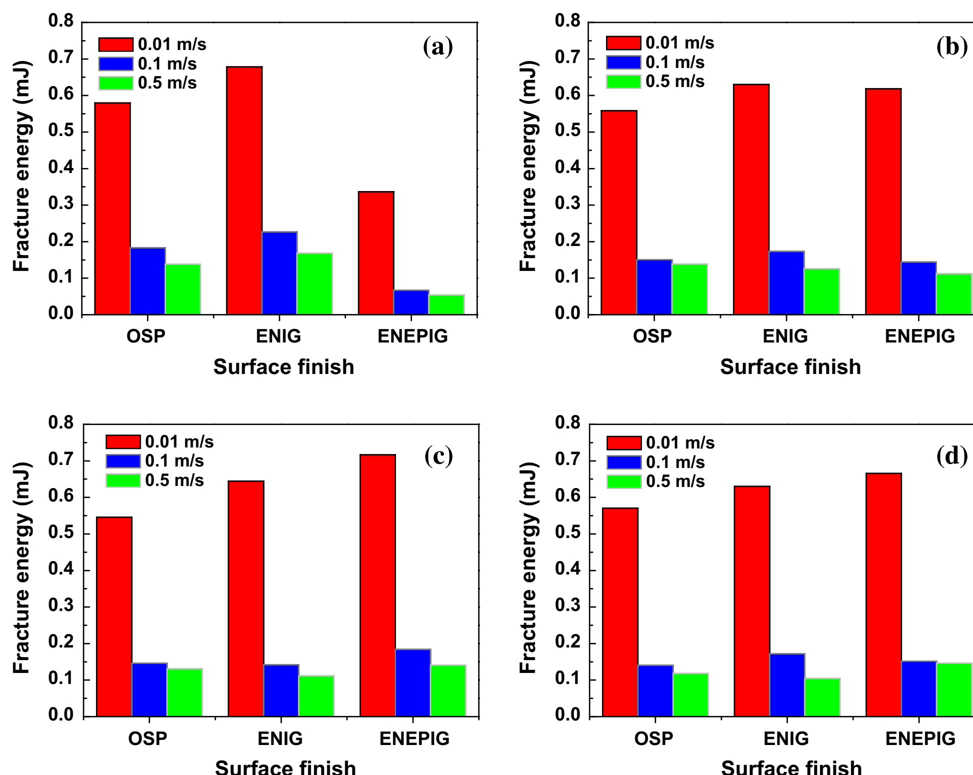

Fig. 15 Fracture energy variation according to surface finish and shear speed: reflowed for **a** 45 s, **b** 80 s, **c** 30 min, and **d** 1 h

4 Conclusions

In this study, we investigated the interfacial reactions and joint reliability of Sn–58Bi solder with three different surface finishes, namely, OSP, ENIG, and ENEPIG. We successfully identified a relationship between interfacial reaction behavior and mechanical reliability of the three solder joints. In the case of the OSP surface finish, Cu_6Sn_5 IMC was initially formed at the interface, and additional Cu_3Sn IMC formed at the interface between the Cu_6Sn_5 layer and Cu substrate during prolonged reflow reactions. Relatively thin and continuous Ni_3Sn_4 IMC layers formed at the Sn–58Bi/ENIG interface. In the case of the ENEPIG substrate, the interfacial IMCs were sequentially changed during reflowing for up to 1 h at 180 °C in the following order: $(Pd,Ni)Sn_4$, $(Pd,Ni)Sn_4 + Ni_3Sn_4$, and Ni_3Sn_4. Compared to the Cu_6Sn_5 IMC on the OSP-finished Cu substrate, the Ni_3Sn_4 IMCs on the ENIG and ENEPIG substrates were much thinner. Furthermore, the thicknesses of the Ni_3Sn_4 IMC and Ni_3P layers in the Sn–58Bi/ENEPIG joint were thicker than those in the Sn–58Bi/ENIG joint, which was attributed to the different interfacial IMC morphologies owing to direct contact between liquid solder and Ni–P substrate during the reflow reaction. The growth rates of the interfacial IMC layers and consumption rates of the Ni–P layer were closely related to the interfacial microstructure and morphology. The layer-type well-attached interfacial IMCs had advantages with respect to IMC growth rate and Ni–P consumption rate. In the high-speed shear test, the shear force increased with increasing shear speed, mainly due to the high strain-rate and work-hardening effect of the solder alloys. In addition, the Sn–58Bi/ENEPIG joint with $(Pd,Ni)Sn_4$ IMC had a relatively low shear force. In contrast, the Sn–58Bi/ENEPIG joint with Ni_3Sn_4 IMC was robust, and had a high shear force value. However, the surface finish material did not significantly affect the shear force of the Sn–58Bi solder joints under high-speed shear loading.

References

1. Y.D. Jeon, K.W. Paik, K.S. Bok, W.S. Choi, C.L. Cho, J. Electron. Mater. **31**, 520–528 (2002)
2. S.W. Jeong, J.H. Kim, H.M. Lee, J. Electron. Mater. **33**, 1530–1544 (2004)
3. G. Milad, D. Gudeczauskas, Metal Finish. **104**, 33–36 (2006)
4. G. Milad, M. Orduz, Metal Finish. **105**, 25–28 (2007)
5. J.W. Yoon, S.B. Jung, J. Alloys Compd. **396**, 122–127 (2005)
6. Y.C. Sohn, J. Yu, J. Mater. Res. **20**, 1931–1934 (2005)
7. J.W. Yoon, S.B. Jung, Surf. Coat. Technol. **200**, 4440–4447 (2006)
8. J.W. Yoon, B.I. Noh, S.B. Jung, IEEE Trans. Compon. Packag. Technol. **33**, 64–70 (2010)

9. W.H. Wu, H.L. Chung, N. Lee, R. Peng, C.E. Ho, in *Proceedings of the 5th International Microsystems Packaging Assembly and Circuits Technology Conference (IMPACT)* (2010), pp. 1–4
10. J.W. Yoon, B.I. Noh, J.H. Yoon, H.B. Kang, S.B. Jung, J. Alloys Compd. **509**, L153–L156 (2011)
11. B. Kobe, N.S. McIntyre, Acta Mater. **50**, 4667–4676 (2002)
12. C.T. Lu, H.W. Tseng, C.H. Chang, T.S. Huang, C.Y. Liu, Appl. Phys. Lett. **96**, 232103 (2010)
13. J.W. Yoon, M.K. Ko, B.I. Noh, S.B. Jung, Microelectron. Reliab. **53**, 2036–2042 (2013)
14. Y.W. Yen, P.H. Tsai, Y.K. Fang, S.C. Lo, Y.P. Hsieh, C. Lee, J. Alloys Compd. **503**, 25–30 (2010)
15. Z. Liu, J. Cai, Q. Wang, X. He, Y. Chen, J. Electron. Mater. **43**, 3341–3350 (2014)
16. R. Zhang, F. Guo, J. Liu, H. Shen, F. Tai, J. Electron. Mater. **38**, 241–251 (2009)
17. J.O. Suh, K.N. Tu, G.V. Lutsenko, A.M. Gusak, Acta Mater. **56**, 1075–1083 (2008)
18. W.K. Choi, S.Y. Jang, J.H. Kim, K.W. Paik, H.M. Lee, J. Mater. Res. **17**, 597–599 (2002)
19. G.Y. Jang, J.W. Lee, J.G. Duh, J. Electron. Mater. **33**, 1103–1110 (2004)
20. H.B. Kang, J.H. Bae, J.W. Lee, M.H. Park, J.W. Yoon, S.B. Jung, C.W. Yang, J. Electron. Mater. **37**, 84–89 (2008)
21. Y.K. Jee, J. Yu, Y.H. Ko, J. Mater. Res. **22**, 2776–2784 (2007)
22. C.E. Ho, W. Gierlotka, S.W. Lin, J. Mater. Res. **25**, 2078–2081 (2010)
23. S.P. Peng, D. Lin, C.E. Ho, in *Proceedings of the 4th International Microsystems Packaging Assembly and Circuits Technology Conference (IMPACT)* (2009), pp. 505–508
24. S.P. Peng, W.H. Wu, C.E. Ho, Y.M. Huang, J. Alloys Compd. **493**, 431–437 (2010)
25. H.S. Chun, J.W. Yoon, S.B. Jung, J. Alloys Compd. **439**, 91–96 (2007)
26. J.W. Yoon, B.I. Noh, S.B. Jung, J. Electron. Mater. **40**, 1950–1955 (2011)
27. J.W. Kim, S.B. Jung, Metal Mater. Int. **16**, 7–12 (2010)